

Ab initio zone-center phonons in LiTaO₃: comparison to LiNbO₃

V. Caciuc

Universität Osnabrück – Fachbereich Physik, D-49069 Osnabrück, Germany

A. V. Postnikov

Gerhard Mercator University Duisburg – Theoretical Low-Temperature Physics, D-47048 Duisburg, Germany

(May 11, 2001)

The four A_1 -TO Γ phonon frequencies in lithium tantalate are calculated in the frozen-phonon approach from first principles using the full-potential linearized augmented plane wave method. A good agreement with the experimental data available is found for all modes; reliable displacement pattern of different modes becomes available from the calculated eigenvectors. The Raman spectra recorded for A_1 modes in LiNbO₃ exhibit a counter-intuitive softening of the A_1 -TO₃ mode frequency with respect to that measured in LiTaO₃. We explain this behavior by a comparatively harder oxygen rotation in LiTaO₃ and discuss other differences in lattice dynamics of two materials, notably delocalization of Ta and Li contributions over more than one corresponding mode in LiTaO₃, differently from the situation in lithium niobate. The Li isotope shift is predicted in the calculation.

63.20.-e, 71.15.Ap, 77.84.Dy

INTRODUCTION

The ferroelectric materials LiNbO₃ and LiTaO₃ have been intensively studied over years due to their promising applications in non-linear optical and electro-optical devices – see Ref. 1 for a review on relevant properties of these materials. Both compounds possess rhombohedral space group $R3c$ (C_{3v}^6) and have 10 atoms in the unit cell. They remain ferroelectric up to quite high transition temperatures: T_C amounts to 1480 K in LiNbO₃ (that is probably the highest ferroelectric transition temperature so far known) and 950 K in LiTaO₃.

Due to low symmetry and large number of atoms in the unit cell, the first-principles studies of LiNbO₃ and LiTaO₃ proceed not so fast as, e.g., for perovskite-type ferroelectric compounds, KNbO₃ and KTaO₃ (the latter is an incipient ferroelectric, where the transition can be induced by uniaxial pressure, or by doping). Soon after first *ab initio* studies of electronic structure², the analysis of the aspects of ferroelectric instability by Inbar and Cohen^{3,4} was illuminating in that they emphasized an importance of oxygen-rotating mode in the ferroelectric transition. Earlier, the z -displacement of Li ions out of the oxygen planes was believed to be the essence of the ferroelectric transformation. Inbar and Cohen demonstrated that the energy profile in the para- to ferroelectric transition (studied along the path connecting experimentally determined end-point structures) is very similar in both substances. As a possible explanation of the difference in the T_C values, they guessed that the zone-boundary behavior may be found to be different in LiNbO₃ and LiTaO₃. This assumption has not yet been tested.

While we do not access exactly this topic in the present study, we believe that the analysis of phonon properties, even at zone center, can give a clue to understanding different behavior of LiNbO₃ and LiTaO₃. Due to the complexity of structure, the analysis of lattice vibrations

in experiment was in part contradictory, and in what regards theory only few calculations have been done. For LiNbO₃ we calculated earlier^{5,6} the frequencies and eigenvectors of TO- Γ phonons, based on a precision total-energy fit in the multidimensional (up to dimension 9, for the E block) space of symmetry coordinates. Parlinski *et al.*⁷ calculated the phonon dispersion over the full Brillouin zone of LiNbO₃, using the direct method and the Fourier transformation of force constants sampled by displacing individual atoms in a 80-atoms ($2 \times 2 \times 2$) supercell. Semiempirical phonon calculations (i.e., fitting the model parameters to experimentally measured frequencies) have been done by Repelin *et al.*⁸ for both LiNbO₃ and LiTaO₃. We are not aware of any first-principles phonon calculations for LiTaO₃.

On the experimental side, at least for the A_1 modes there is very good agreement between different measurements in what regards vibration frequencies – see Table I. Comparing them with the frequencies for LiNbO₃ shown in the same table one can note that the frequencies are lower in LiTaO₃ for all modes but one, the TO₃. Whereas the mode softening can be – at least qualitatively – intuitively related to larger mass of Ta, and different degree of softening of different modes – to different participation of Ta (Nb) in them, the hardening of the TO₃ mode on going from LiNbO₃ to LiTaO₃ is clearly counter-intuitive and can be only traced to the differences in electronic properties.

The aim of the present study is to provide an *ab initio* description of zone-center A_1 -TO phonons in LiTaO₃ and discuss them in comparison with corresponding phonons in LiNbO₃, thus outlining small but important differences in electronic properties in these materials. In the following we briefly outline the details of calculation and proceed with the discussion of phonon frequencies and eigenvectors.

TABLE I. A_1 -TO phonon frequencies in LiNbO_3 and LiTaO_3

	exp. LiNbO_3		exp. LiTaO_3			LiTaO_3	${}^6\text{LiTaO}_3$	$(\text{Li}^{m_{\text{Nb}}}\text{TaO}_3)$
Ref.	[9]	[10]	[11]	[12]	[8]		present calculation	
TO_1	252	206	203	206	201	194	199	(197)
TO_2	275	253	252	253	253	242	252	(261)
TO_3	332	356	356	356	356	360	361	(360)
TO_4	632	600	597	597	597	599	599	(602)

TABLE II. Internal coordinates in LiTaO_3 (experiment and theoretical optimization)

	Ta		Li			O			
Experiment: Ref. 17	0	0	0	0	0	0.279	0.050	0.344	0.069
Present calculation	0	0	0	0	0	0.282	0.049	0.343	0.071

CALCULATION SCHEME

Our frozen-phonon calculation was based on precision all-electron total-energy calculations with the use of full-potential linearized augmented plane waves method, as implemented in the WIEN97 code¹³. The local orbitals extension according to Ref. 14 has been used for a better description of Ta $5s$ and $5p$, Li $1s$ and O $2s$ states. The muffin-tin radii chosen were 1.88 a.u. for Ta and 1.65 a.u. for Li and O. The exchange-correlation energy has been treated in the local density approximation as parametrized by Perdew and Wang¹⁵.

The Brillouin zone integrations were carried out by the improved tetrahedron method¹⁶ on a $4 \times 4 \times 4$ special k -points mesh which generated 13 k points in the irreducible Brillouin zone. When using a denser $6 \times 6 \times 6$ k -mesh (32 irreducible k -points), we found a difference in the total-energy trends less than 1 mRy, negligible for the analysis of the lattice dynamics in the scale of energy variations discussed below. The planewave cutoff parameter $R_{\text{min}}K_{\text{max}}$ for the basis was set to 9.5, that resulted in, on the average, 2313 basis functions for each k -point; the cutoff parameter G_{max} for the charge density expansion was 12.0, i.e., these cutoff values had to be set to higher values than in our earlier calculations for LiNbO_3 ⁶ in order to achieve acceptable convergence. The optimized lattice parameters turn out to be $a=5.1274$ a.u. and $c=13.7033$ a.u., giving the error of -2% in the volume and -0.1% in the c/a ratio as compared to experimental values $a=5.1543$, $c=13.7835$ a.u.¹⁷. The subsequent calculations analyzing the atomic displacements have been performed with the lattice parameters fixed at their experimental values.

As regards the frozen-phonon formalism as such, it is known since long¹⁸ and has been successfully applied to many systems. This approach is physically transparent, and its accuracy is easy to control. The bottleneck of the method is the necessity to calculate the forces (or, alternatively, expansion coefficients of the total energy over individual atomic displacements) for many trial geometries, in order to map the total energy near equilibrium to quadratic or, if necessary, higher or-

ders in displacements. This rapidly makes the computation unpractical for moderately large systems, and/or those with reduced symmetry (where many vibrational degrees of freedom mix in the same irreducible representation). Earlier, we succeeded in calculating zone-center phonons for, at the largest, the 9-dimensional E -block of LiNbO_3 ⁶, adding progressively data points (i.e., trial geometries) that would refine normal coordinates, as the latter emerge more and more clearly in the course of calculations. In the present study, our concern is the 4-dimensional A_1 block of the crystal vibrations in LiTaO_3 , for which we make a comparison with previously obtained LiNbO_3 data⁶. In order to obtain a reliable mapping of the total energy we included 170 different geometries in our calculation. The optimized internal coordinates as they emerge from the four-dimensional total-energy fit are shown in Table II. They serve as reference point for all displacements discussed later on.

RESULTS

For the set of four symmetry coordinates $S_{1...4}$ chosen in terms of individual Cartesian displacements as specified in Ref. 6 for LiNbO_3 , the diagonalization of the dynamical matrix yields four normal coordinates as follows:

$$\begin{pmatrix} S_{\text{TO}_1} \\ S_{\text{TO}_2} \\ S_{\text{TO}_3} \\ S_{\text{TO}_4} \end{pmatrix} = \begin{pmatrix} -2.145 & -1.189 & -0.457 & 1.120 \\ 3.915 & -1.371 & 0.131 & 0.265 \\ -0.253 & 0.356 & -0.350 & 1.563 \\ -1.039 & -0.157 & 1.153 & 0.373 \end{pmatrix} \begin{pmatrix} S_1 \\ S_2 \\ S_3 \\ S_4 \end{pmatrix}.$$

These normal coordinates serve as abscissa in Fig. 1 that visualizes corresponding cuts of the total energy hypersurface. The number of trial configurations allows to perform a stable 4th order polynomial fit, also shown in Fig. 1. It is obvious that the corrections to the 2d order fit are small and not always physically sane, i.e. not all leading 4th order terms are positive. In other words, all four A_1 -TO modes, according to our calculation, are essentially harmonic, much more so than it was the case for their counterparts in LiNbO_3 (see a similar analysis in Ref. 6). Another ‘‘empirical’’ justification of this

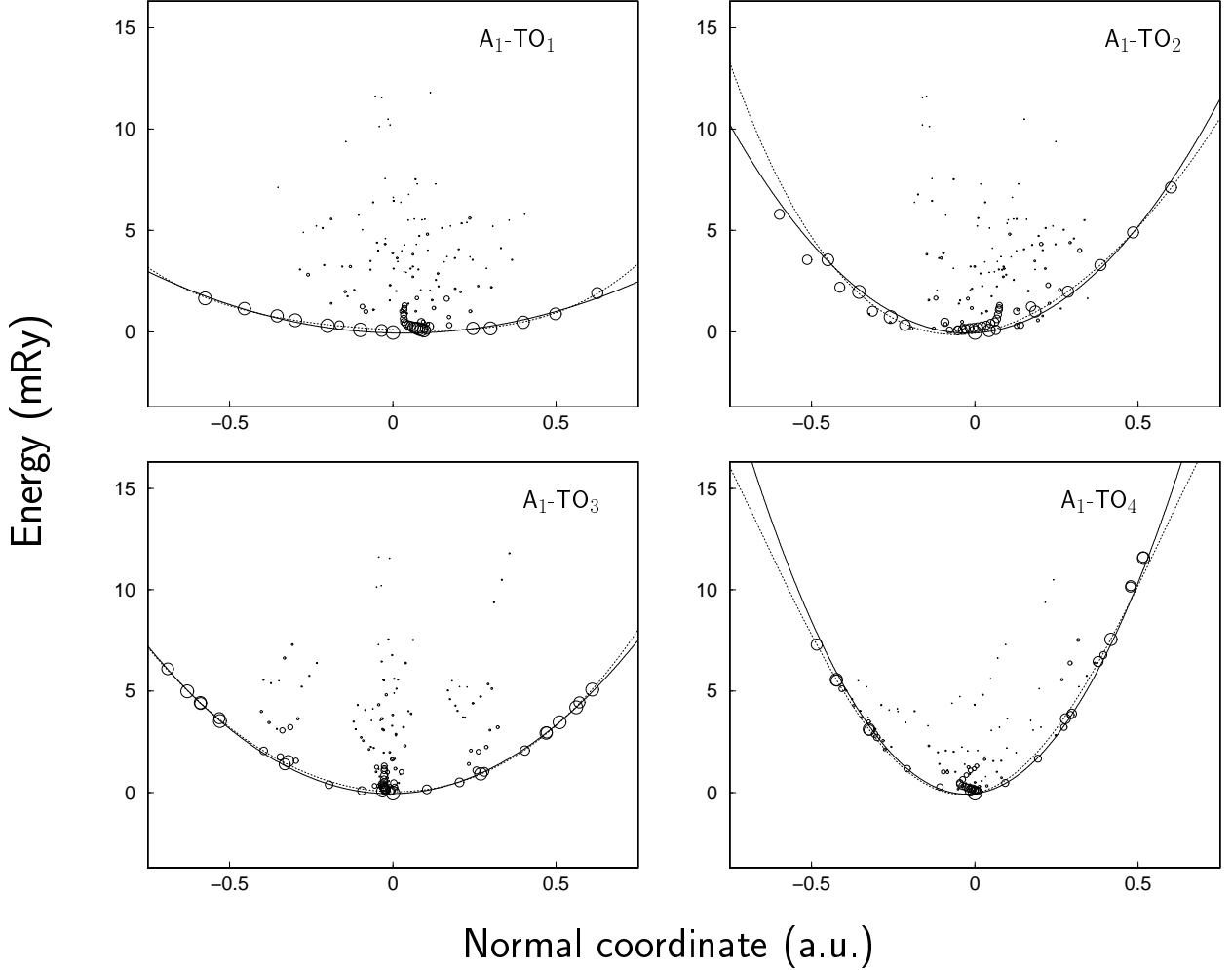


FIG. 1. The cut of the total-energy fit along the directions of normal displacements in the four-dimensional space of symmetry coordinates corresponding to the A_1 symmetry. The circles' sizes are inversely proportional to the distances of corresponding data points from the direction of normal displacement. Solid lines represent the 2d-order polynomial fit, dashed lines – the 4th order fit.

fact is much better agreement of measured and calculated (harmonic) frequencies than it was the case in LiNbO_3 (see Table I). The largest difference ($7 - 12 \text{ cm}^{-1}$) between our calculation and experiment occurs for the TO_1 and TO_2 modes, with experimental values higher, as it could be usually expected due to anharmonicity. For two other modes, the agreement between experiment and theory is almost perfect, as consistent with neat parabolic fit through data points along the directions of these two normal coordinates in Fig. 1. In LiNbO_3 , the difference between theory and experiment amounted to 46 cm^{-1} (TO_1) and 50 cm^{-1} (TO_4 mode), both these modes being considerably unharmonic judging on their corresponding total energy profiles. In the following, we discuss the composition of different modes and address the “anomalous” TO_3 mode (i.e., that is harder in tantalate than in

niobate) in some detail.

Since the LiNbO_3 and LiTaO_3 are in many aspects so similar, we would like, when discussing their phonon frequencies, to know whether the existing differences are mostly due to higher tantalum mass, or to variations in corresponding force constants. The simplest illustration of the effect of mass is the calculation of frequencies with the mass of Nb atom taken instead of that of Ta; the results are given in the last column of Table I. Unexpectedly enough, the frequency noticeably increases in the course of such substitution solely for the TO_2 mode; for three other modes, even for the TO_1 (the mainly “Nb” mode in LiNbO_3 , see Ref. 6) the effect is negligible, consistently with much smaller Ta contribution in corresponding eigenvectors (see below).

Such “Ta isotope” effect roughly accounts for the half

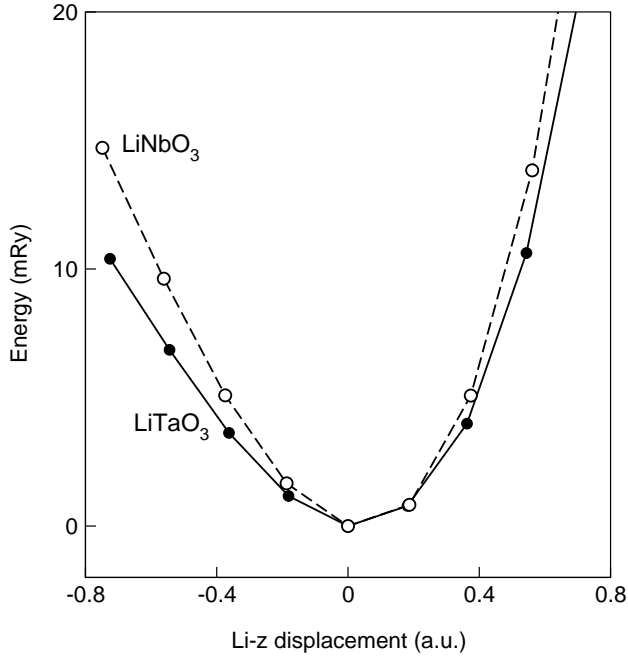


FIG. 2. Potential energy profile associated with Li z -displacements in A_1 - TO_3 mode of LiNbO_3 (LNO) and LiTaO_3 (LTO). Positive movements shorten the distance between Li and O ions, while the negative movements shorten that between Li and Nb(Ta) ions.

of the TO_2 frequency shift in $\text{Li}(\text{Ta} \rightarrow \text{Nb})\text{O}_3$; the rest can only come from the steeper potential well associated with Li z -displacement in LiNbO_3 . The corresponding total energy profile is shown in Fig. 2. The reason for the “softness” of the LiTaO_3 lattice with respect to such Li-only vibration can be simply a somehow larger interatomic spacing, as illustrated by Table III. It was already emphasized earlier by Inbar and Cohen³ that Li always remains quite well ionized in both tantalate and niobate and that no effects of dynamical covalency that would lead to coupling of oxygen and lithium motions are seen in these materials.

Let us now turn to calculated eigenvectors shown in Table IV in the hexagonal setting. The “prototype” oxygen atom is that whose coordinates are given in Table II; from its eigenvector components (x, y, z) the components related to other oxygen atoms can be reconstructed as $(\bar{y}, x - y, z)$, $(y - x, \bar{x}, z)$, $(y - x, y, \frac{1}{2} + z)$, $(\bar{y}, \bar{x}, \frac{1}{2} + z)$, $(x, x - y, \frac{1}{2} + z)$. For comparison, the eigenvector compo-

TABLE III. Distances (a.u.) to nearest neighbors and next nearest neighbors of transition metal and oxygen to lithium atom in LiNbO_3 and LiTaO_3

	$\text{Nb}(\text{Ta})_{\text{NN}}$	$\text{Nb}(\text{Ta})_{\text{NNN}}$	O_{NN}	O_{NNN}
LiNbO_3	5.595	7.159	3.799	4.276
LiTaO_3	5.669	7.355	3.848	4.367

nents for LiNbO_3 are also given; their transformation to the Cartesian system according to

$$\begin{pmatrix} x \\ y \\ z \end{pmatrix} = \begin{pmatrix} 0 & \sqrt{3}/2 & 0 \\ 1 & -1/2 & 0 \\ 0 & 0 & c/a \end{pmatrix} \begin{pmatrix} x_h \\ y_h \\ z_h \end{pmatrix}.$$

recovers the eigenvectors for LiNbO_3 as given in in Ref. 6. As in LiNbO_3 , the heavy transition-metal ion contributes mostly to the two low-frequency modes. In the softest one, it vibrates along with Li against the oxygen octahedra which are only slightly tilted in this process (the tilting originates merely from a crystal structure frustration, as was discussed in Ref. 3). This is the ferroelectric mode, frozen down from the paraelectric phase, near its “freezing point”. The TO_2 mode includes lithium vibration against both transition-metal and oxygen sublattices; two other modes are too high for efficiently resonating with transition-metal vibrations.

The Li contribution exhibits some differences in two systems. To make these differences, somehow obscured in center-of-mass related eigenvectors, more clear, we show in Table V pure (not scaled with masses) vibration patterns of the four modes, relative to the heaviest Nb(Ta) atom and normalized so that the displacement of (any) second heaviest constituent atom, i.e. oxygen, is 1. Whereas in LiNbO_3 the lithium vibration is essentially confined to the TO_2 mode (that alone is affected by the Li isotope shift^{12,5}), in LiTaO_3 the Li effect on the TO_1 and TO_3 modes is also not negligible, with possible implications for their frequencies on Li isotope doping. The frequencies calculated with reduced Li mass are shown in Table I. The maximal frequency shift (for the TO_2 mode) reduces from 19 cm^{-1} in LiNbO_3 to 10 cm^{-1} in LiTaO_3 . We guess that the Li isotope shift of the TO_1 mode is probably still large enough to be detected experimentally. Moreover, the Li-related phonon density of states, if ever calculated similarly to how it was done in Ref. 7 for LiNbO_3 , must certainly become spread off lower and higher frequencies.

The second largest contribution of Li occurs, for both materials, in the eigenvector of the TO_1 mode. Even if it is much smaller (relative to the center of masses) in niobate, the displacement pattern of this mode is oxygen z -vibration against both the heaviest atom *and* lithium, so that the Li–O stretching is anyway present. Here again the hardening of the Li-related potential well on changing from LiTaO_3 to LiNbO_3 plays a role: the mere change of mass produces only a minor effect in elevating the calculated (harmonic) frequency to 208 cm^{-1} in niobate⁶; the strong anharmonicity of this mode contributes the rest up to its measured frequency of 252 cm^{-1} .

The two hardest modes exhibit but negligible Nb(Ta) contribution in both materials; the effect of Li z -displacement is also quite reduced (although remains noticeable in LiTaO_3), so we have here two almost exclusively O_{xy} patterns, almost identical in tantalate and niobate. These two modes are, correspondingly, a nearly

TABLE IV. Eigenvectors of TO phonons in LiNbO₃ and LiTaO₃ in the hexagonal setting

	LiTaO ₃					LiNbO ₃				
	Ta	Li	O		Nb	Li	O			
TO ₁	0.060	0.168	(0.096	0.132	-0.104)	0.143	0.035	(0.036	0.085	-0.123)
TO ₂	0.109	-0.191	(-0.047	0.038	-0.080)	0.068	-0.254	(0.015	-0.014	0.001)
TO ₃	-0.007	0.051	(-0.441	-0.101	-0.003)	0.007	-0.001	(-0.463	-0.156	-0.006)
TO ₄	0.029	0.022	(-0.127	-0.440	-0.037)	0.023	0.015	(-0.082	-0.437	-0.022)

 TABLE V. Cartesian coordinates at equilibrium (top line) and displacement patterns in the four A₁ modes of LiNbO₃ and LiTaO₃, relative to the Ta(Nb) atom and with the oxygen displacements normalized to 1.

	Li		O1		O2			O3		
	<i>z</i>	<i>x</i>	<i>y</i>	<i>z</i>	<i>x</i>	<i>y</i>	<i>z</i>	<i>x</i>	<i>y</i>	<i>z</i>
	LiTaO ₃									
coord.	0.282 <i>c</i>	-0.280 <i>a</i>	0.122 <i>a</i>	0.405 <i>c</i>	0.034 <i>a</i>	-0.304 <i>a</i>	0.405 <i>c</i>	0.246 <i>a</i>	0.181 <i>a</i>	0.405 <i>c</i>
TO ₁	0.75	0.13	-0.04	-0.38	-0.04	0.13	-0.38	-0.10	-0.10	-0.38
TO ₂	-1.14	0.04	0.09	-0.40	-0.10	-0.01	-0.40	0.05	-0.08	-0.40
TO ₃	0.22	-0.09	0.40	-0.00	-0.30	-0.28	-0.00	0.39	-0.12	-0.00
TO ₄	0.07	-0.38	-0.09	-0.12	0.27	-0.28	-0.12	0.11	0.37	-0.12
	LiNbO ₃									
coord.	0.281 <i>c</i>	-0.278 <i>a</i>	0.127 <i>a</i>	0.401 <i>c</i>	0.029 <i>a</i>	-0.304 <i>a</i>	0.401 <i>c</i>	0.249 <i>a</i>	0.177 <i>a</i>	0.401 <i>c</i>
TO ₁	-0.01	0.06	0.01	-0.40	-0.04	0.05	-0.40	-0.03	-0.06	-0.40
TO ₂	-6.17	-0.07	-0.05	-0.40	0.07	-0.03	-0.40	-0.01	0.08	-0.40
TO ₃	-0.01	-0.14	0.38	-0.02	-0.27	-0.31	-0.02	0.40	-0.08	-0.02
TO ₄	0.04	-0.38	-0.14	-0.08	0.31	-0.26	-0.08	0.07	0.39	-0.08

rigid rotation of oxygen octahedra hosting Nb atoms and the bending of the octahedra (rotation of three top atoms against the three bottom ones). The “top view” of corresponding distortions has been shown in Fig. 2 of Ref. 5 for LiNbO₃. What is noteworthy about TO₃ and TO₄ modes is that for *both* of them the calculated frequency is by ~ 16 cm⁻¹ higher in tantalate. Then, the anharmonicity of TO₄ in LiNbO₃ (but not in LiTaO₃) accounts for a considerable increase of experimental frequency in the niobate. The TO₃ mode is well harmonic in both materials, so that the relation between phonon frequencies in niobate and tantalate as predicted by the calculation is essentially retained in reality. Since the TO₄ mode in both materials is almost free of transition-atom and lithium contributions, the last panel of Fig. 1 and the corresponding energy profile in Fig. 1 of Ref. 6 exhibit essentially the effect of bending of oxygen octahedra and give a fair indication that the latter are more rigid in LiTaO₃.

An analogy to that can be found in cubic perovskites: among many calculations done by date of zone-center phonons in KNbO₃ and KTaO₃ by comparable techniques^{19–22}, the calculated frequencies of two hardest modes, that correspond to different distortions of oxygen octahedra, are higher in tantalate than in niobate. The experimental situation confirms this at least for the TO₄ mode (the TO₃ of the T_{2u} symmetry is Raman and infrared silent in cubic perovskite, so that its measurements are not numerous; corresponding frequencies any anyway quite close in KNbO₃ and KTaO₃). The possible origin

of this seemingly systematic trend can be sought for either in a slightly increased lattice spacing of tantalates – that would however probably have an opposite effect on the oxygen rigidity, if at all – or in a slight difference in the degree of covalency. The latter guess gets support from the analysis of the dynamical matrix corresponding to the soft-mode motion (i.e., also including the oxygen tilting) by Inbar and Cohen⁴. They have shown that the “full” O–O elements of this matrix are larger in LiTaO₃, whereas the relation between Madelung contributions to the dynamical matrix (i.e., those assuming nominal ionic charges) is opposite.

The aspects of relative covalency of tantalates and niobates are influenced by several factors; discussions to the point can be found in Ref. 20 on perovskites and in Ref. 4 on our present systems of interest. Summarizing, the covalency seems to be higher in tantalates, judging by a slightly wider valence band and a stronger dispersion of certain bands, that is seemingly related to less localized d -function of tantalum. A possible link to the stiffness of oxygen octahedra may be that higher covalency enhances interaction between lattice-dynamical degrees of freedom, softening the softest modes and hardening the hardest. Indeed, the span of TO-frequencies, at least in the harmonic approximation, seems to be typically broader in tantalates. Different degree of anharmonicity of different modes may complicate the experimental situation.

CONCLUSION

We extended our previous frozen-phonon analysis of zone center-TO phonons in lithium niobate over lithium tantalate. For all A_1 modes quite good agreement was found between the experimental and calculated phonon frequencies, indicating, differently from LiNbO_3 , a quite harmonic nature of all four modes. In spite of large similarity in crystal structure and electronic properties, the phonon eigenvectors show certain differences in both systems. Specifically, the Li contribution, that was in LiNbO_3 only noticeable in the single TO_2 mode, now spreads over TO_1 to TO_3 modes. One can expect the Li isotope shift in LiTaO_3 to become less pronounced but affecting these three modes. Li displacement experiences a softer potential well in LiTaO_3 , due to more expanded lattice, that lowers the frequencies of Li-dependent modes. The contribution of the transition metal ion affects the TO_2 mode more than TO_1 , contrary to the case in LiNbO_3 . Contrary to the effect on Li, the rotational modes of oxygen octahedra are noticeably hardened in LiTaO_3 , indicating a more stiff oxygen network. Due to this, a higher frequency of the TO_3 mode in tantalate is explained. For the TO_4 mode, the harmonic part of which also gets harder in LiTaO_3 , the experimental situation is reversed only due to a strong anharmonicity of this mode in LiNbO_3 .

ACKNOWLEDGMENTS

The work was supported by the German Research Society (graduate college "Microstructure of oxidic crystals"). The authors are grateful to G. Borstel for introduction to the subject. A.V.P. appreciates stimulating discussions with P. Bourson, M. Fontana and V. Vikhnin.

- ⁹ A. Ridah, M. D. Fontana, and P. Bourson, *Phys. Rev. B* **56**, 5967 (1997).
- ¹⁰ X. Yang, G. Lan, B. Li, and H. Wang, *Phys. Status Solidi B* **142**, 287 (1987).
- ¹¹ C. Raptis, *Phys. Rev. B* **38**, 10007 (1988).
- ¹² S. Kojima, *Jpn. J. Appl. Phys.* **32**, 4373 (1993).
- ¹³ P. Blaha, K. Schwarz, and J. Luitz, WIEN97, Vienna University of Technology, 1997, improved and updated Unix version of the original copyrighted WIEN-code, which was published by P. Blaha, K. Schwarz, P. Sorantin, and S. B. Trickey, in *Comput. Phys. Commun.* **59**, 339 (1990).
- ¹⁴ D. J. Singh, *Phys. Rev. B* **43**, 6388 (1991).
- ¹⁵ J. P. Perdew and Y. Wang, *Phys. Rev. B* **45**, 13244 (1992).
- ¹⁶ P. E. Blöchl, O. Jepsen, and O. K. Andersen, *Phys. Rev. B* **49**, 16223 (1994).
- ¹⁷ S. C. Abrahams, E. Buehler, W. C. Hamilton and S. C. Laplaca, *J. Phys. Chem. Solids* **34**, 521 (1973).
- ¹⁸ K. Kunc and R. M. Martin, *Phys. Rev. B* **24**, 2311 (1981); *Phys. Rev. Lett.* **48**, 406 (1982).
- ¹⁹ D. J. Singh and L. L. Boyer, *Ferroelectrics* **136**, 95 (1992).
- ²⁰ D. J. Singh, *Phys. Rev. B* **53**, 176 (1996).
- ²¹ A. V. Postnikov, T. Neumann, and G. Borstel, *Phys. Rev. B* **50**, 758 (1994).
- ²² R. Yu and H. Krakauer, *Phys. Rev. Lett.* **74**, 4067 (1995).

¹ E. Krätzig and O. F. Schirmer, in *Photorefractive Materials and Their Applications I*, ed. by P. Günter and J.-P. Huignard (Springer, Berlin, Heidelberg 1988) p.131.

² W. Y. Ching, Z.-Q. Gu, and Y.-N. Xu, *Phys. Rev. B* **50**, 1992 (1994).

³ I. Inbar and R. E. Cohen, *Ferroelectrics* **164**, 45 (1995); *Ferroelectrics* **194**, 83 (1997).

⁴ I. Inbar and R. E. Cohen, *Phys. Rev. B* **53**, 1193 (1996).

⁵ A. V. Postnikov, V. Caciuc, and G. Borstel, *J. Phys. Chem. Solids* **61**, 295 (2000).

⁶ V. Caciuc, A. V. Postnikov, and G. Borstel, *Phys. Rev. B* **61**, 8806 (2000).

⁷ K. Parlinski, Z. Q. Li, and Y. Kawazoe, *Phys. Rev. B* **61**, 272 (2000).

⁸ Y. Repelin, E. Husson, F. Bennani, and C. Proust, *J. Phys. Chem. Solids* **60**, 819 (1999).